ANASEN: the Array for Nuclear Astrophysics and Structure with Exotic Nuclei

E. Koshchiy[a,c], J.C. Blackmon[b], G.V. Rogachev[a,c], I. Wiedenhöver[c], L. Baby[c], P. Barber[c], D.W. Bardayan[d], J. Belarge[c], D. Caussyn[c], E.D. Johnson[c], K. Kemper[c], A.N. Kuchera[c], L.E. Linhardt[b], K.T. Macon[b], M. Matoš[d], B.S. Rasco[b], D. Santiago-Gonzalez[b,c]

[a] *Texas A&M University, Department of Physics & Astronomy and Cyclotron Institute, College Station, TX 77843, USA*
[b] *Louisiana State University, Department of Physics & Astronomy, Baton Rouge, LA 70803, USA*
[c] *Florida State University, Department of Physics, Tallahassee, FL 32306, USA*
[d] *Physics Division, Oak Ridge National Laboratory, Oak Ridge, TN 37831, USA*

Abstract

An active target detector array, ANASEN, has been developed for nuclear reaction studies with rare isotope beams at low energies. It aims at measurements of the excitation functions for proton and α- particle elastic and inelastic scattering and direct measurements of (α,p) reactions with exotic nuclei in inverse kinematics. ANASEN is composed of three types of charged particle detectors. The length of the active area is 340 mm and the total covered area is 1300 cm^2 (almost 3π steradian solid angle coverage) providing high efficiency for experiments with low intensity radioactive beams. A mix of 78 conventional electronics channels (for Proportional Counter and CsI- detectors) and 480 dedicated high-density ASICs electronics channels for the silicon detector are used for readout.

PACS 29.40.Cs Gas-filled counters: ionization chambers, proportional, and avalanche counters 29.40.Gx Tracking and position-sensitive detectors

Keywords: Active gas target; Charge particles detection; Multiwire position sensitive proportional counter; Silicon-strip detectors; CsI(Tl) detectors; Radioactive beams; Inverse kinematic

1. Introduction

Reactions involving radioactive nuclei play an important role in stellar explosions, but limited experimental information is available due to difficulties in producing and studying radioactive nuclei. The progress in development of radioactive nuclear beams (both in-flight and re-accelerated) provides greater access to these unstable isotopes, but the typical beam intensities are still much lower compared to stable beam facilities. That's why more efficient and selective techniques and devices are required to be able to study many important reactions of astrophysical interests.

For instance, novae and X-ray bursts are the most common stellar explosions in the Galaxy and result from thermonuclear explosions on the surface of compact stars in binary systems. The study of these processes is important to understand the structure and evolution of white dwarfs and neutron stars, as well as accretion and mixing mechanisms that play a crucial role in many astrophysical environments. So far our understanding of novae and X-ray bursts is limited in part by a lack of nuclear data regarding reactions that play a key role in the explosions, such as (p,γ), (p,α) and (α,p). The rates of these reactions are often determined by the properties of low-energy resonances that correspond to nuclear energy levels just above the proton (or α) threshold in corresponding compound nuclei. The large uncertainties that exist in most of these reaction rates are due to unknown properties of these low-energy resonances.

The Array for Nuclear Astrophysics and Structure with Exotic Nuclei (ANASEN), developed in a collaboration between Florida State University (FSU), Louisiana State University (LSU), and Texas A&M University (TAMU) was designed primarily to be used in measurements of (α,p) reactions and of proton and alpha elastic and inelastic scattering in inverse kinematic using radioactive ion beams and thick targets. The main philosophy was to construct a detector that employs the advantages of an extended gas target, has vertex reconstruction capability and can still be used with very high intensity radioactive beams (up to 10^9 pps) that will soon become available at the Facility for Radioactive Ion Beams (FRIB) at Michigan State University.

Measurements of proton elastic and inelastic scattering will indirectly determine the properties (energies, spin-parities and proton partial widths) of some of the nuclear levels that are important in (p,γ) and (α,p) reactions. While direct measurements of (p,γ) reactions are needed for the most important cases, such measurements are especially difficult, requiring both high radioactive beam intensities and substantial experimental infrastructure (e.g., large recoil separators). More straightforward studies like proton elastic and inelastic scattering are needed first to provide a basic picture of the energy level structure of these nuclei and to help identify what are, in fact, the most important resonances. Since such reaction rates depend exponentially on the resonance energy, such indirect studies can substantially reduce uncertainties in the nuclear reaction rates.

ANASEN is targeted towards measurements with the RESOLUT radioactive ion beam facility at the John D. Fox Supercon-

Email addresses: koshchiy@comp.tamu.edu (E. Koshchiy), rogachev@tamu.edu (G.V. Rogachev)

ducting Accelerator Laboratory at FSU ([1]) and with the new re-accelerated beam facility (ReA3) at the National Superconducting Cyclotron Laboratory at Michigan State University.

ANASEN has cylindrical geometry, that is well suited for high efficiency inverse kinematics reaction studies. The target gas is used as an active gas for a cylindrical gas proportional counter array that provides position information on the reaction products at one point close to the beam axis. The light recoils (typically protons or α-particles) are detected by a position sensitive silicon-strip detector array backed with CsI. The particular geometry of the gas detector electrodes and the silicon detector array allows reconstruction of the track of each reaction product on an event-by-event basis to allow the reaction, center-of-mass energy, and final state to be determined. The use of CsI allows high-energy protons to be detected as well.

ANASEN achieves its high sensitivity and efficiency by combining a high areal-density target with a large solid angle detector coverage, amounting to around $\sim 3\pi$ sr. Simultaneously, it excludes the region of high ionization density induced by the beam, which allows for relatively high-intensity radioactive beams to be used. Its design allows for an efficient measurement of excitation functions over a large dynamic range of cross sections. These are the properties needed for the spectroscopy of astrophysical resonances and measurements of (α, p) reactions.

The TRIUMF Annular Chamber for Tracking and Identification of Charged Particles (TACTIC) aims toward a similar goal [2] but has very different design.

2. Array design

A schematic cross-section view of ANASEN is shown in Fig. 1.

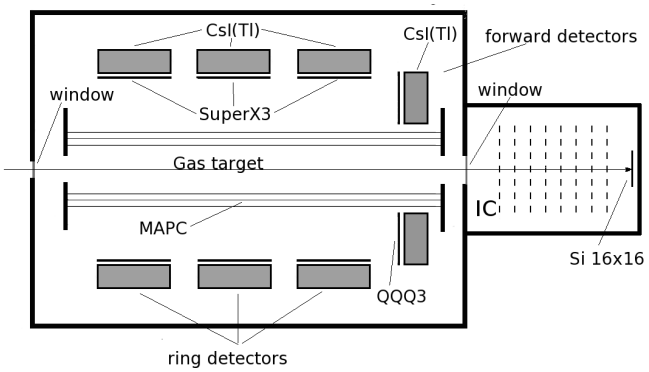

Figure 1: Schematic cross-section view of ANASEN

The detector follows a cylindrical design pattern, with three layers of detector systems surrounding the beam axis. The innermost layer is a multi-anode position-sensitive proportional counter (MAPC), which enables the *active-target* mode. At radii of 88 mm from the beam- axis, three identical rings of 12 rectangular Silicon strip detectors are surrounding the MAPC. For detecting particles at laboratory angles near 90°, a most effective "barrel" geometry that involves detectors arranged parallel to the incident beam direction (and more perpendicular to track of detected particles) has been selected. Angles near 90° are more important for measurements of (α,p)-reactions with an extended gas target to make it easier to reconstruct events that are emitted more perpendicular to the incident beam direction (a notable recent implementation of this detector geometry is ORRUBA ([3]) which has been developed for measurements of (d,p) reactions). The Silicon detectors of the Super-X3 design are backed by CsI(Tl) crystals of trapezoidal-bar geometry.

In addition to the "ring"- assemblies, the beam-forward angles are covered by an annular configuration of four QQQ3-design silicon strip detectors. Each QQQ3 detector is backed by the set of 4 segment shaped CsI(Tl) detectors. The "forward" assembly covers a wide angular range of polar angles from about 3° (at the maximum feasible length of 70 cm) up to $> 70°$ in the lab frame, if the reaction occurs close to the forward QQQ3 detectors. The ANASEN elements are mounted inside a cylindrical stainless steel scattering chamber of 60 cm diameter and 100 cm length. An entrance window separates the ANASEN volume from the beamline vacuum. Depending on the experiment, a window as thin as 2 micron (Aramica, Asahi Chemical, Japan or Havar foil for the rare isotope beams that have intensity exceeding 10^{7-8} ions/sec) or thicker can be used. For example, the 7.5 micron Kapton (DuPont, USA) window with diameter of 10 mm allows to run safely at the gas pressure up to about 2000 Torr (see, for example: [4]) and take the most beams of interest with the beam current up to 100 pA.

A basic pump-out pressure at the level of 10^{-6} Torr is provided by assembly of turbo and scroll pumps (Leybold).

In addition to the detectors described above, a fast-counting ionization chamber (IC) can be attached to ANASEN at $\theta_{lab} = 0°$. The IC is an ancillary detector for experiments that require detection of the heavy recoils but it can also be used for beam tuning and diagnostics of beam composition. The IC consist of 20 parallel copper planes with 1mm spaced wire grid, supported by four isolated rods. The diameter of the entrance window is 6.4 cm. The chamber can be partitioned into several independent segments, providing for additional particle ID when needed. The three-segment configuration was used in the first experiments. The IC's maximum counting rate is about 10^5 pps. Some details can be found in [5].

3. Individual array components

The general view of the main components of ANASEN is shown in Fig. 2.

3.1. Multi-Anode Proportional Counter (MAPC)

The two basic requirements for the MAPC design are: i) high gain to be able to detect high energy protons that lose less than 10 keV in the active volume of the MAPC cell, and ii) good position resolution (within few mm range) for tracking. Both

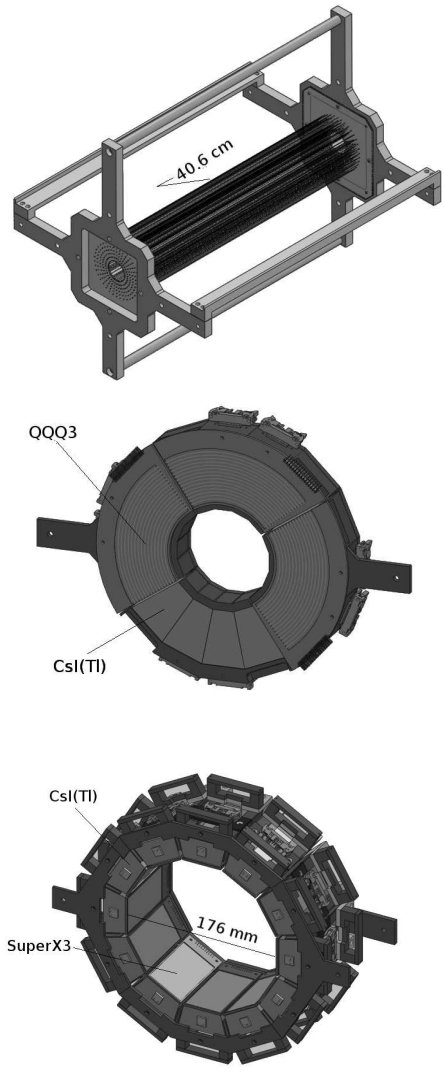

Figure 2: ANASEN elements: Top Panel: Multi-Anode position sensitive Proportional Counter (MAPC); Central panel: Forward detector array (one of QQQ3 Si detector has been removed in order to show the CsI(Tl) detectors behind it) ; Bottom panel: Ring array comprised of 12 Super-X3 backed by CsI(Tl).

requirements can be satisfied by proper selection of the anode material and detector geometry.

The optimized configuration of the proportional counter was determined using the computer code GARFIELD-9 [6]. Following the results of the simulation, the proportional counter was made with anodes arranged cylindrically with respect to the beam axis at the radial distance of 30 mm. Each anode is surrounded by 8 grounded cathodes, to form a trapezoidal pattern Faraday cage. This arrangement makes 19 independent "hexagonal" proportional counter cells with an effective thickness of 12.5 mm, as is shown in Fig. 3a and 3b. The outer and inner guard rings (Fig. 3) are used to suppress delta electrons produced in the area outside of the cells from drifting into the cells.

Several different techniques of position sensitivity were reviewed in [7], the simplest one of which is charge division over a resistive anode wire, with examples discussed in Refs. [8–10]. We chose this method for ANASEN, which made the choice of the anode wire material critical, with few materials providing the mechanical stability at the small diameter for the required proportional counter gain, combined with the high wire resistance for good position resolution. Alloy materials, such as Nichrom (0.8Ni+0.2Cr), Iron Alloy 875 (0.72Fe+0.225Cr+0.055Al), High Resistance Alloy (0.55Fe+0.375Cr+0.075Al) were considered, but show low resistances of 150-250 Ω/cm, while the Carbon- coated Quartz that has the highest resistance proved to be not durable enough. The solution was found in Carbon fiber filaments, whose performance was studied in [11, 12], and which has been used in several proportional counters [13–15]. Following the design of Ref.[7] a Carbon fiber material (Panex-35, ZOLTEK Co) with 7 μm thickness was chosen as the anode material for ANASEN.

For the cathode wires, two different materials were tested. The prototype was made from Silver- plated Copper with 75 μm diameter. We experienced that the wires stretched with time, which led to instabilities. Instead, Gold- plated Tungsten wire of the same diameter was selected for the final design.

The total length of the active area of MAPC is 430 mm.

Pre-treated with a solvent in an ultrasonic bath, Carbon fiber filaments were pasted with conductive paint (Silver Print 2, GC Electronics) to the Nickel- plated Copper pins. The filaments were stretched between the two end plates (printed circuit boards), mounted to the Aluminum frame (see Fig. 2, MAPC) forming the body of wall-less counter. The qualified filaments that passed the mechanical strength test (0.08 N) were soldered to the end-plates. The mounting tension on the individual carbon fiber was about 0.05 N.

Gold-plated Tungsten cathode wires and guard-ring electrodes were spring-loaded at the upstream end-plate of the detector with a tension of around 0.35 N. The ends of the cathode wires were soldered to the MAPC board and grounded. The inner and outer guard-rings are mechanically attached in the same way, but they have independent feed circuits. As a result of the combined wire tensions, the total force on the end plates is about 30 N.

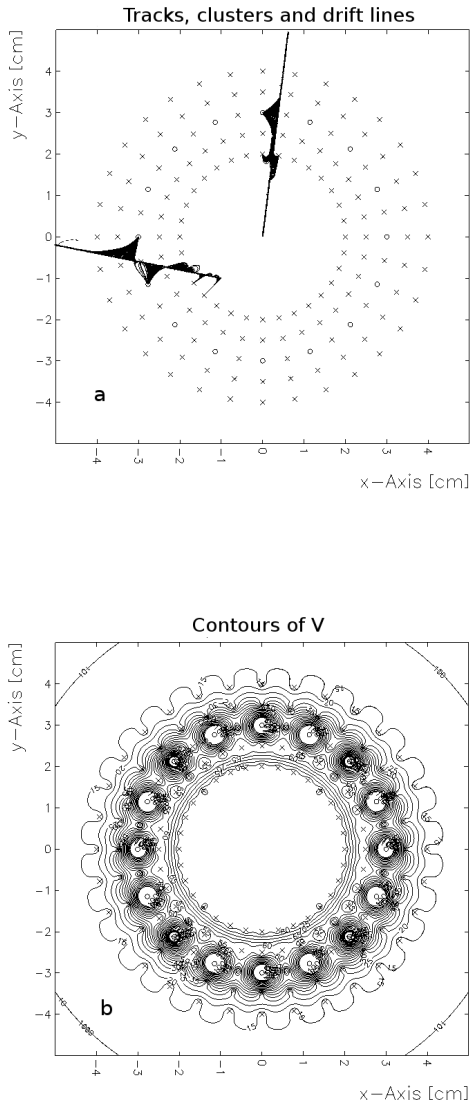

Figure 3: GARFIELD simulations **a**: cross section of multiwire proportional counter (○ – anodes; × – cathodes and "guard"- electrodes) with electron drift lines from the tracks of 5 MeV protons; Methane, P=300 torr); **b**: Contours of electric field (V_{anode}=500V, both cathodes and "guard" electrodes - grounded)

3.2. Silicon detectors

Surrounding the proportional counter is a barrel of silicon detectors that was developed in conjunction with Micron Semiconductor. Silicon strip detectors were chosen for ANASEN because a large area can be covered while achieving good energy and position resolution. The Super X3 model is a double-sided, 75x40 mm silicon-strip resistive layer detector, segmented on both front and back sides. The Super-X3 design was adapted from the X3 detectors, used for ORRUBA [3]. The difference is that the back ohmic faces of the detector are segmented into four 18x40 mm^2 strips that are used to determine the energy, independent of position, and assist with position calibration of the resistive front strips. The front (junction) face of Super-X3 detector has four resistive strips that are 75 mm long and 10 mm wide. There are 12 signals, 8 front and 4 back, for each of these detectors. The Super X3 detector design is shown in Fig. 4.

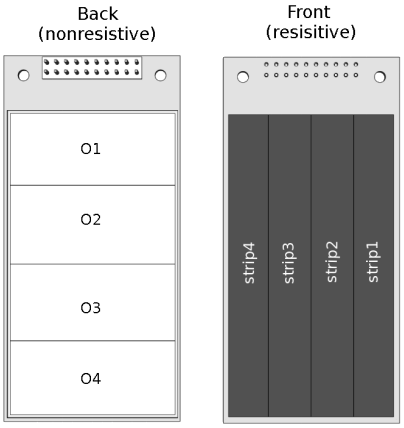

Figure 4: SuperX3 detector

Annular double sided silicon detectors were designed to cover a large fraction of the angular range for forward angles. The active area of each double-sided quadrant detector extends between radial distance of 55 mm to 99 mm. The forward detector set covers an area of 210 cm^2, with the largest radius possible using 4 pieces of silicon (using 15 cm wafer technology). The QQQ3 detector has 16 front rings and an inner a active area of 55 mm and 99 mm, respectively, 16 back segments with 4 quadrant detectors creating a complete set. The front rings and the back segments are shown in Fig. 5. Both of the segmented silicon detectors, Super X3 and QQQ3, are 1000-μm- thick. This silicon thickness corresponds to the range of 12 MeV protons at normal incidence.

3.3. CsI(Tl) scintillator array

The outer layer of the array was composed from trapezoid shaped 26-mm- thick CsI(Tl) scintillator from SCIONIX. These detectors are used to identify and measure residual energy of particles that can penetrate through the silicon array (typically only high energy protons and deuterons).

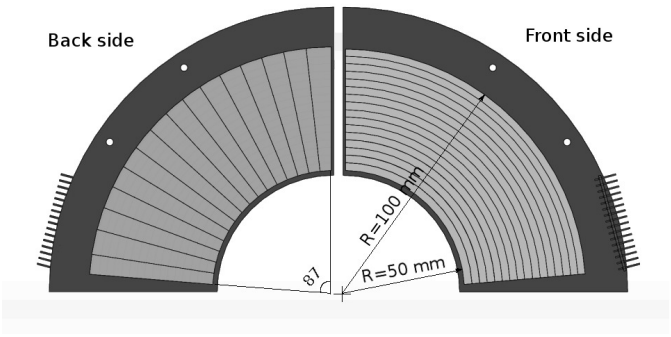

Figure 5: QQQ3 detector

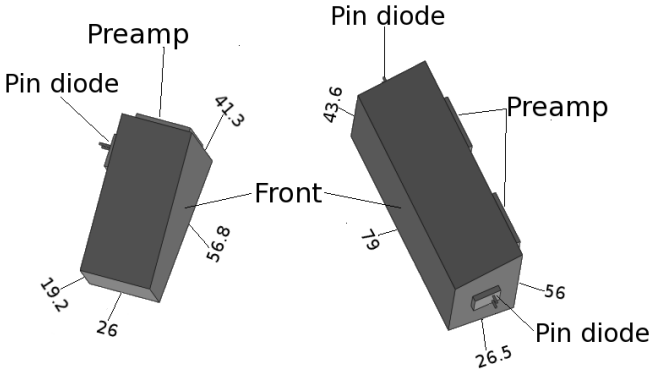

Figure 6: CAD rendering of CsI(Tl) detectors, Type I [left] and Type II [right].

There are two different geometries of CsI(Tl) detectors used in ANASEN, shown in Fig. 6. Type I detectors have been designed so that an arrangement of 16 crystals can fully cover the forward silicon detectors in pie shaped segments, four for each QQQ3 detector. Each CsI(Tl) crystal is wrapped in 2-μm- thick aluminized mylar, and has a built-on preamplifier which is read out by a single Hamamatsu 20x20 cm^2 S3204 PIN diode. Type II CsI(Tl) detector has been designed to fit behind the Super-X3 detectors, covering the same solid angle.

The face of the Type II crystal covers the back side of the SuperX3 silicon detector and extends 1.5 mm beyond its active area. It tapers outward with radius on the sides at an angle of 13.5°. This geometry ensures that if a recoil particle that is scattered at 90° with respect to the beam axis hits a SuperX3 Si detector then it cannot escape the CsI crystal. However, for shallow trajectories the escape is still possible near the upstream and downstream edges and has to be taken into account in the analysis. Scintillation from Type II detectors are read out by two pin-diodes from opposite sides of crystals, allowing to determine both total energy and Z- position of scintillation (along the beam axis). Under optimal noise conditions, the energy resolution with a ^{241}Am source is 5% for the Type I geometry crystals and 8% for the Type II. It is limited by variation in the efficiency of light collection due to geometry and uniformity of scintillator light output throughout the volume. It is natural that the larger scintillator crystals (Type II) have worse energy resolution on average.

3.4. Electronics

With the combination of the multichannel proportional counter, silicon detectors, and CsI(Tl) detectors, there are over 500 channels of electronics in the full configuration of ANASEN. To deal with this high channel count in a cost effective manner, ANASEN utilizes Application-Specific Integrated Circuits (ASICs) of the HINP16C design by Washington University [16] in combination with conventional MESYTEC electronics (for MAPC and Cs(I) detectors –136 channels total).

Each HINP16C ASIC handles the pulse-shaping, timing, and triggering of 16 channels of data. The system as a whole has 2 ASICs HINP16C chips per board, with 16 boards in the system, handling up to 512 channels in one motherboard. Analog signals from all channels are multiplexed into XLM flash ADCs. ANASEN uses 2 motherboards and XLM modules. A VME-USB Wiener interface is used to send the collected digitized data from the front end processor using NSCL DAQ ([17]). External preamplifiers are used to optimize the energy resolution and dynamic range. A custom 72-channel preamplifier system for Si detectors has been developed based on the Indiana University's LASSA preamplifier chip; with a gain of 27 mV/MeV and a 30 μs fall time that matches the shaping of the HINP16C ASICs [18].

With a complete ANASEN implementation comprising 560 signals from Si detectors, handling a high-density of electronics without losing resolution becomes a priority. We designed a circuit board feed-through to map 6 Super X3 detectors through regular density Insulation Displacement Connector (IDC) to high density IDC cabling to get the signals out of the vacuum. Another vacuum-tight circuit board was designed to feed 64 channels of two QQQ3-detectors with the same preamplifier box.

3.5. Gas handling system

It is well known (see, for example [19, 20]), that the gain of the proportional counter without gas flow changes significantly over time due to the gas deterioration. The origin of this effect may be an accumulation of electro-negative additives from polymers covering flat cables connecting detectors and construction elements, beam induced gas deterioration and the layering effect of gas mixtures. The latest is distinct in helium/carbon-dioxide gas mixture which is the working media for investigation of (α,p)- reactions. For the active gas-target mode, the gas handling system has to fit the requirements of high accuracy and stability to keep operating pressure and gas flow during runs of up to a few weeks, and meet safety specification for use of flammable gases (Hydrogen/Deuterium, Methane, Iso-Butane). The gas/vacuum handling system for ANASEN is shown schematically in Fig. 7.

The pressure and gas flow is controlled by an integrated pressure controller with πPC-99 (MKS instruments) mass flow me-

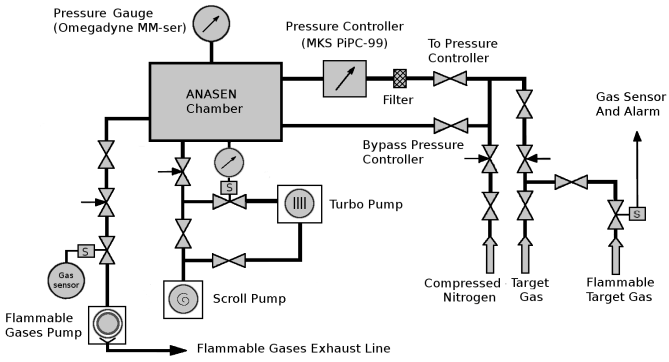

Figure 7: The scheme of gas the handling system.

ter. It was configured to be capable of controlling pressure in the range of 30 Torr to 1200 Torr with the accuracy of ±1% through TCP/IP protocol. A high accuracy (±0.05%) gas independent absolute pressure transducer MM series (OMEGA Engineering) is set for the complementary monitoring of the gas pressure. An extra pump is installed for evacuation of flammable gases away from laboratory building through the specific exhaust line. The gas sensor shuts the input line valve and activates an alarm signal in case of exceeding the maximum allowable content level of flammable gases. As a result of tests it was found that the gas flow on the level greater than 100 sccm is sufficient to maintain stable operation of the MAPC.

Because the current configuration does not support recycling, the gas is stored in empty cylinders for further offline cleaning during experiments with isotope enriched target gases (deuterium, for example). During long lasting experiments, the ANASEN chamber is refilled with fresh deuterium in certain time intervals. The reliability of the system with respect to the gas pressure stability has been demonstrated during several 3 - 4 week long runs.

The performance of the position sensitive proportional counter depends on the energy and type of radiation, counter geometry, composition and pressure of working gas and applied anode voltage (gas amplification) [10, 19]. For example, the position sensitive proportional counters with 7 μm diameter Carbon fiber as resistive anode was extensively tested in [7] and references therein (mostly, for X-ray emission spectroscopy). It was shown that for the P-10 gas mixtures (90%Ar+ 10%CH_4) the minimum position resolution of 0.15 mm can be obtained with the highest pressure, i.e. 10 atm.

The gas composition and pressure are determined by the specific conditions of the experiment. Therefore the original tests were conducted with a standard P-10 gas to compare it with specific gases that could be used as target gases for ANASEN experiments (H_2, D_2, CH_4, He+CO_2) at the pressure in a range of 100 to 1200 Torr.

4. Testing and calibration of detectors

4.1. Multi-anode proportional counter

Two different techniques have been employed for both energy and position calibration. Initially, the MAPC was tested and calibrated independently from other ANASEN elements with an ^{241}Am α-source (intrinsic calibration), and then the final calibration was performed in the complete ANASEN setup with the silicon array using the ^{210}Po needle α-source (see Fig. 8).

For the intrinsic calibration a standard ^{241}Am α- source was mounted outside of the MAPC at the distance of 65 mm from its axis. The α- source was collimated by two pairs of slits so that the size of an irradiated area at the most distant anode does not exceed 1 mm. An exact positioning (mechanical accuracy of about 0.5 mm) of the α-source along the anode wires was run by a micrometer-motion mechanism. This technique allows to test and calibrate independently all anodes simultaneously. A positive high voltage was applied to both ends of anode wires. Signals from both ends of the MAPC wires are decoupled from the high voltage by capacitors and read out by charge sensitive preamplifiers and sent to the ADC through a spectroscopic amplifier (all electronics are fabricated by MESYTEC). Because of the wide energy range of detected reaction products, a MPR-LOG series preamplifier was used for the proportional counter readout. It provides a linear range that covers about 70% of the total, and the remaining 30% covers the high energy end logarithmically.

A pulser calibration of all electronic channels was made to provide the gain matching. This is especially important for determination of event position location at the MAPC anode and further recovery of vertex, because a position reconstruction technique is based on charge division method: X=(Up-Dn)/(Up+Dn), where X - position of signal with respect to the Upstream (Up) and Downstream (Dn) end of the resistive anode. Later this “Intrinsic” position is converted to ”Global” 3D coordinates of total ANASEN setup (see below). The results of the position calibration for one of anodes is shown in the Fig. 9.

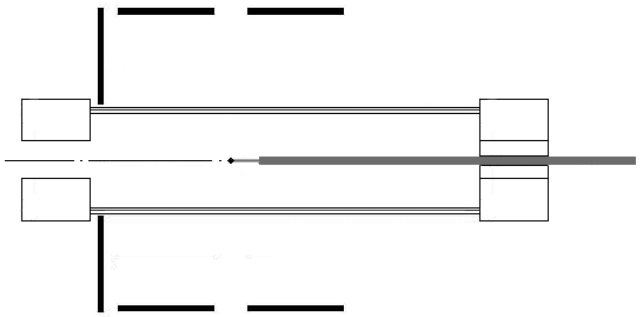

Figure 8: Schematic view of the testing setup. A sliding “needle” α- source placed at the ANASEN axis.

Extensive information on the properties of different gases suitable for proportional counters and drift chambers were accumulated (see, for example [19] end Ref. there). Typically the different mixtures of noble gases (helium, argon) with small additions of hydrocarbons (methane, butane) or organic (ethyl- or methyl- alcohol) provide the highest gas amplification. The resolution of the proportional counter (both energy and position) depends on gas composition, pressure and applied voltage. Be-

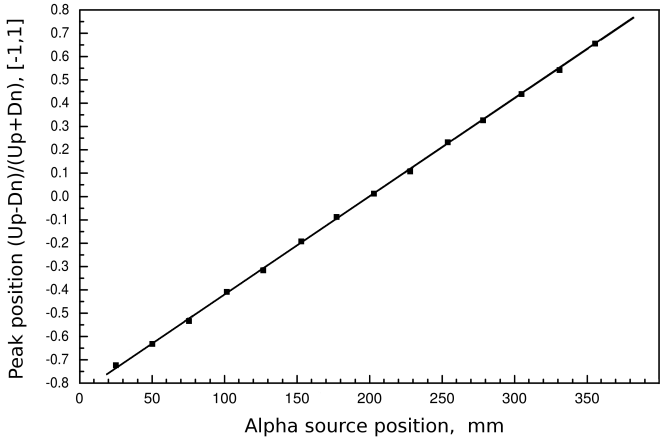

Figure 9: MAPC position calibration. Gas: P-10, P=30 torr. Solid squares - experiment. The measurement errors are within the size of squares.

cause ANASEN is an active target detector, it limits the selection of an appropriate gas and defines the working conditions.

The desired target gases for ANASEN are those that contain hydrogen and helium isotopes. Pure H_2 seems to be the best option for experiments with protons, but in this case high pressure has to be achieved to slow down or stop incident ions inside ANASEN, especially at high beam energy. Usually hydrocarbon gases (methane, iso-butane) can be used for proton scattering experiments. They combine characteristics which qualify them as a target gas in active target detector: high hydrogen concentration, sufficient stopping power and high gas amplification at low voltage. If helium is the desired target then it has to be quenched to reduce fluorescence from electron de-excitation that is competitive with the ionization process [21, 22]. The dependence of the position resolution on anode voltage is shown in Figs. 10 and 11 for different gas mixtures.

4.2. Super X3

As mentioned above, the Super X3 detectors have a total of 12 channels, where channels 0-3 correspond to the ohmic back segments and channels 4-11 to the downstream (4-7) and upstream (8-11) sides of the 4 resistive front strips. The energy is obtained from the back segments and the position from the front strips. Signals from a high-precision pulse generator are fed directly into the preamplifier in order to extract the electronics offset. In this section we explain the energy and position calibration procedures for the Super X3 detectors. More details on these procedures can be found in [23].

The energy calibration of each Super X3 detector is done in two steps: 1) align all the back-channel signals, 2) get the absolute energy calibration. Both steps require data from an alpha source such as ^{228}Th. In step 1, a reference channel is selected (usually one with high statistics). Then, proportional constants are found for the rest of the back channels so that the centroids of their peaks match the ones of the reference channel. In step 2, the energy spectra of all back channels is combined from which the energy calibration coefficients can be extracted, see Fig. 12. The typical energy resolution was found to be ~ 50 keV (FWHM).

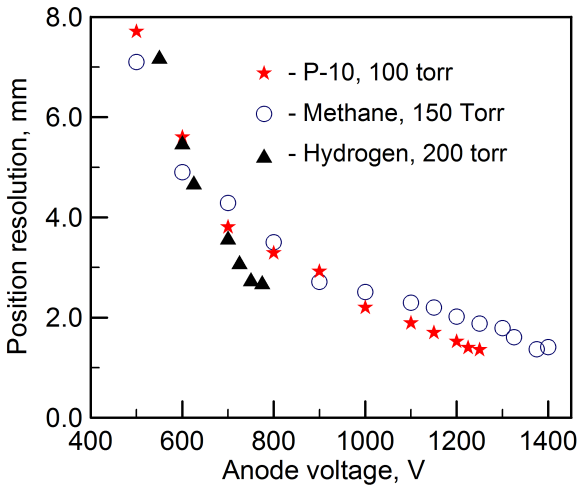

Figure 10: Position resolution as a function of anode bias for different gas mixtures

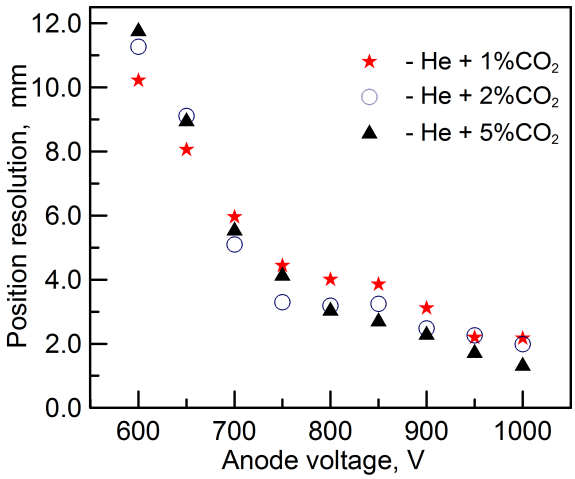

Figure 11: Position resolution as a function of anode bias for helium gas with different concentrations of CO_2 quenching gas

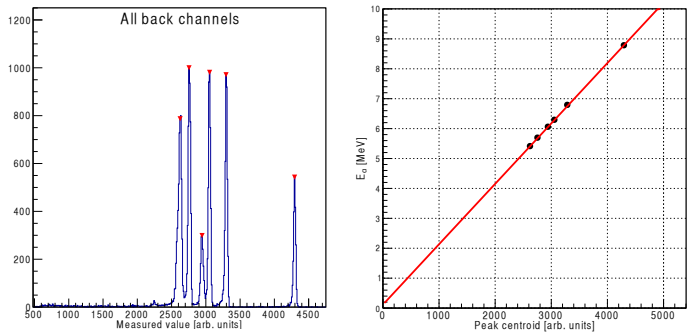

Figure 12: Left: Energy signals measured by a Super X3 detector from a ^{228}Th α source. Right: α particle energy as a function of the centroid of the peaks found in the left spectrum, the red line represents a linear fit.

The position of a hit in the SuperX3 detector is determined using a ratio of the calibrated signals from one side of the front strip to the signal of the back segment: Up (or Down) / Total. The decision on what side of the front strip to be used for a specific event is based on the information of which back segment has fired and allows to always chose the side that received more charge. This procedure is implemented to minimize the effective energy threshold in position measurement.

In order to calibrate the Super X3 internal position to an actual physical length we used data from the charge-sharing events from hits between n-type contacts on the detector. These are particle hits that occur at the border between the two back segments, triggering two back channels with relatively large signals. These hits correspond to about 0.4% of all hits, thus we had to sort large amounts of data to achieve reasonable statistics. Since locations of these regions (three for Super X3) are known, accurate position calibration can be achieved. Fig. 13 shows how the position calibration coefficients are extracted. For 5 MeV α-particles the Super X3 detectors showed a position resolution of 1.2 mm (FWHM).

The energy dependence of the hit position for the charge sharing events in the Super X3 detector is shown in Fig. 14. The plot shows a marked degradation of position resolution for the events with the energy below 2 MeV. This energy threshold was used for the data analysis (see Fig. 13).

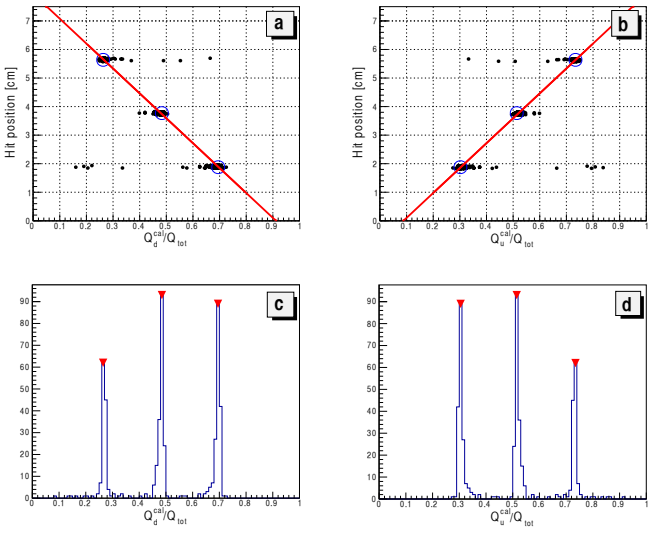

Figure 13: Charge-sharing events from hits between n-type contacts on the detector. (a) and (b) show the position calibration for the down-stream and up-stream sides, respectively. The blue circles represent the position of the centroids of the peaks observed in (c) and (d), which contain the histogram of the down-stream and up-stream calibrated signal over the total signal. The 2 MeV energy cutoff was applied for the back segments (total energy). The data are taken from the ^{17}O(d,p) reaction test run at E(^{17}O) = 55 MeV (see [23]).

5. Test of ANASEN performance in active target mode

The first two commissioning runs were designed to test ANASEN performance in experiments where excitation functions for α elastic scattering and (α,p) reactions are measured. The rare isotope beam of ^{6}He ions was used for the former and the stable ^{14}N beam with intensity degraded down to 10^{7} pps for the later.

5.1. Measurement of excitation function for ^{6}He+α elastic scattering

The ^{6}He+α excitation function was measured recently in [24] in the energy range from 2.0 to 6.0 MeV in c.m. using the AT-TPC active target detector. We have repeated this measurement with ANASEN and extended the measured energy range to 8

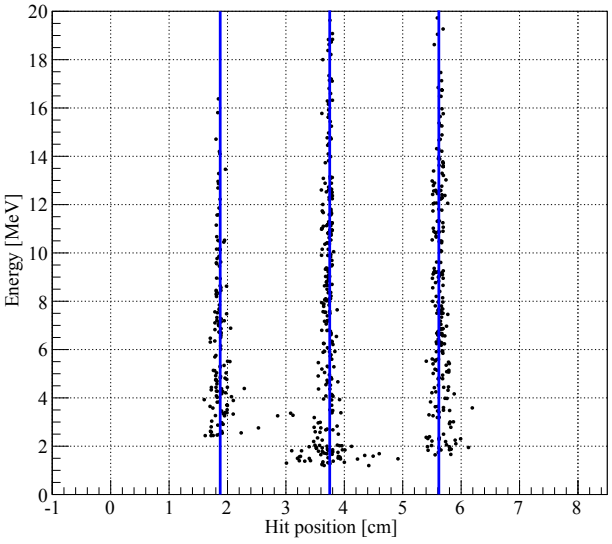

Figure 14: Energy vs position in Super X3 detector for ^{17}O(d,p) reaction at E=55 MeV. The vertical solid lines indicate a position of back segments in Super X3 detector. The dots represent the proton hit position.

MeV in the c.m. In addition to testing the performance of the detector, this experiment had a goal of searching for α-cluster excited states in ^{10}Be at higher excitation energy than in Ref. [24].

A ^{6}He beam was produced at Florida State University's John D. Fox Superconducting Linear Accelerator Laboratory using the radioactive beam facility, RESOLUT ([1]). This beam was produced in flight by a (d,^{3}He) reaction with a stable ^{7}Li beam. The primary beam was accelerated by the tandem and superconducting linear accelerators and impinged on the target gas cell containing deuterium gas cooled to $\approx$ 75 K at a pressure of $\approx$ 350 torr. ^{6}He beams between 7 and 29 MeV entering the chamber were used which covered center-of-mass energies between 2.2 and 8 MeV. We used 7.5 μm thick Kapton entrance foil. The energy loss of the ^{6}He beam in the entrance foil varied from 300 keV for the highest energy to 1 MeV for the lowest energy. Typical intensity of the ^{6}He beam was 10^4 pps. α-particles were the main beam contaminants, contributing at the level of 50-70 % (depending on energy of ^{6}He beam). The events that correspond to the α+α elastic scattering are clearly visible in Fig. 16 as a band above the ^{6}He+α elastic scattering events (indicated by the red gate). We used 8 different energy steps to cover the range of c.m. energies from 2.2 to 8 MeV in c.m. The c.m. energy intervals covered varied from 300 keV for the lowest energy to 1 MeV for the highest energy. To obtain the lowest beam energies (below 19 MeV), plastic degrading foils of various thickness (from 40 μm to 117.5 μm) were placed at the entrance window to ANASEN. The beam energy spread was about 1 % at the highest beam energy (29 MeV) deteriorating to about 15 % at the lowest beam energy due to energy loss straggling and non-uniformity of the degrading foils.

The target gas was a mixture containing helium and carbon dioxide (CO_2) gasses with the CO_2 between 5 and 10 percent of the composition (depending on the energy of ^{6}He beam). The gas pressures ranged from 160 to 700 Torr with the lower pressures used for the lower beam energies.

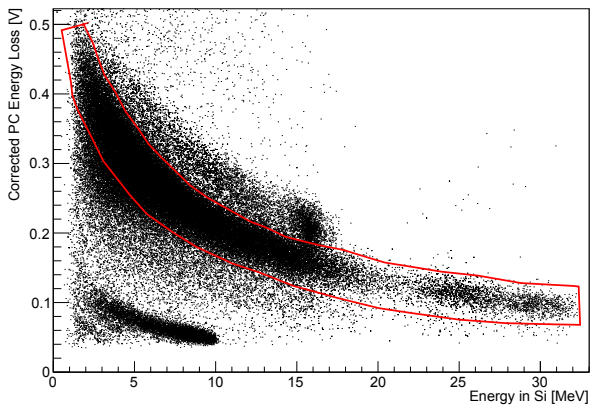

Figure 15: $\Delta E - E$ spectrum with red contour showing the selection of α particles. This figure is adapted from [25].

Events of interest were selected from the $\Delta E - E$ particle identification plots produced from the energy losses in the proportional counter (corrected for the trajectory length in the active volume of the proportional counter cells) and the energy deposited in the Si detectors shown in Fig. 15. By selecting the band corresponding to the scattered α particles the kinematic curves (total energy vs scattering angle) could be determined allowing the ^{6}He+^{4}He reaction channel to be identified as shown in Fig. 16. From the selected reaction of interest, in this case the elastic scattering channel, the differential cross sections were determined. Multiple segments of the excitation function were pieced together to make the continuous spectrum. The angle-integrated spectrum is shown in Fig. 17, compared to the similar spectrum measured in Ref. [24] Details of the analysis procedure can be found in [25]. The overall absolute normalization in this specific run was performed using elastic scattering of ^{6}He on ^{12}C and ^{16}O of the gas mixture CO_2 component. These events have different kinematics than the ^{6}He+α events and can be clearly identified in the 2D energy vs lab. scattering angle scatter plot (similar to Fig. 16) after gaiting on ^{6}He (events above the red gate in Fig. 15). Due to uncertainties in optical model potentials that are used to calculate ^{6}He+^{16}O and ^{6}He+^{12}C elastic scattering cross sections and uncertainties in the composition of the gas mixture the overall uncertainty of the normalization procedure was about 20%. The recent upgrade of ANASEN detector includes a thin scintillator foil and two PMTs in front of the entrance window - making normalization much more accurate and straightforward. This new configuration has already been used in recent run with ReA3 beam at the National Superconducting Cyclotron Laboratory at Michigan State University and will be described in a forthcoming publication. There is a general agreement in the overlapping energy range between Ref. [24] and this work, and the observed deviation can be related to the somewhat different angular range covered and also to the about a factor of two difference in absolute magnitude of the cross section measured at scattering angles below 90° degrees (Fig. 18). The agreement for scattering angles above 90° is nearly perfect (Fig. 19). The

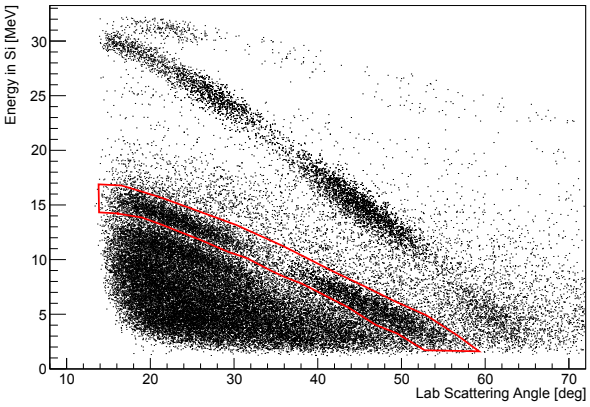

Figure 16: Recoil energy detected in silicon detectors plotted as a function of scattering angle with red contour showing the selection of ^{6}He+α events. The locus above the reg contour corresponds to α+α elastic scattering events and the group below the red contour is ^{6}He+α inelastic scattering and breakup. This figure is adopted from [25].

low energy part of the excitation function (3.0 MeV and below) was obtain using the lowest ^{6}He beam energy of 8 MeV, which had an energy spread of about 1 MeV (FWHM) due to a thick absorber. As a result, energy resolution of the low energy part of the excitation function is 150 keV in c.m., compared to 50 keV at the highest energies.

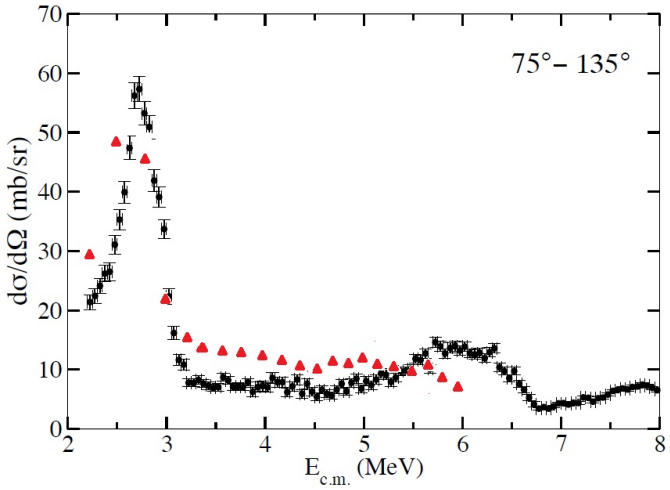

Figure 17: Angle-integrated excitation function for ^{6}He+α elastic scattering. The data from this work are shown by the filled circles. Red triangles - data from [24] (65 -135° in c.m.). The uncertainties shown are purely statistical. This figure is adopted from [25] with addition of data points from cite-SuzukiPRC.

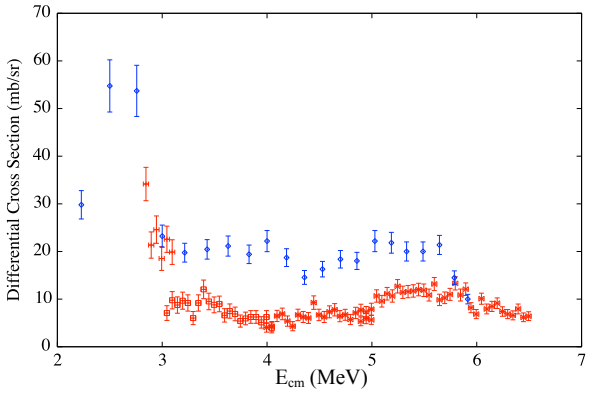

Figure 18: Excitation function for ^{6}He+α elastic scattering at 75°-85° scattering angles. The data from this work are shown in red and data from [24] are in blue (open diamonds). At energies below 3 MeV our data is limited to scattering angles above 80° in c.m. due to effective detector energy threshold.

The dominant feature in the excitation function is the resonance at 2.7 MeV. This state has been previously observed and its spin-parity has been reported to be 3^- [26] and more recently 4^+ [24, 27]. The angular distribution determined from this work is consistent with a $J^\pi = 4^+$ assignment shown by the angular distribution at the peak energy of the 2.7 MeV resonance in Fig. 20. The alternative, 3^- spin-parity assignment, disagrees with the experimental data, as demonstrated by the bottom part of Fig. 20.

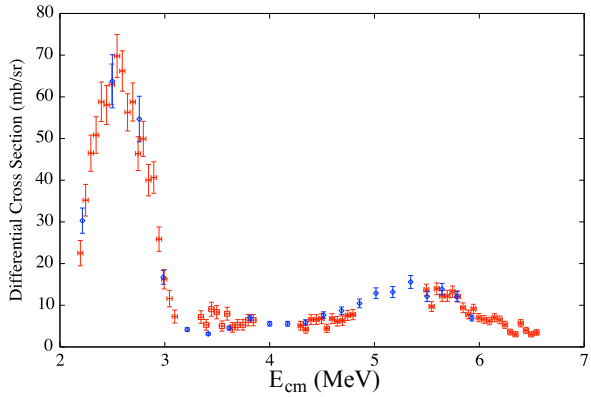

Figure 19: Excitation function for ^{6}He+α elastic scattering at 85°-95° scattering angles. The data from this work are shown in red and data from [24] are in blue (open diamonds).

This peak is considered to be a member of the α:2n:α molecular-type rotational band [27]. Beyond this peak, the excitation function is relatively flat with the exception of a broad structure (≈1000 keV wide) at E$_{c.m.}$ ≈6.1 MeV. The origin of this feature is not clear and further investigation, especially at scattering angles close to 180° in c.m. are necessary to determine if this is the next 6^+ member of the α:2n:α rotational band in ^{10}Be.

5.2. Measurement of excitation function for ^{14}N(α,p) reaction

Measuring excitation functions for the astrophysically relevant (α,p) reactions that involve proton rich nuclei is one of the main goals of ANASEN detector. Therefore, it is important to test the performance of ANASEN for the (α,p) reactions using a well-known case. The excitation function for the ^{14}N(α,p)^{17}O(g.s.) reaction is known from the time-reverse ^{17}O(p,α) measurement Ref. [28] to which the excitation function measured by ANASEN can be compared directly. Of course, the ANASEN measurements have to be performed in inverse kinematics to emulate the rare isotope beam experiment.

The beam of ^{14}N ions with an energy of 35.6 MeV was accelerated by the Tandem at the John D. Fox Superconducting Linear Accelerator Laboratory. A mixture of helium with carbon dioxide gas (99% of He and 1 % of CO_2 by volume) at a pressure of 350 Torr was used for these measurements. The selection of the ^{14}N(α,p)^{17}O(g.s.) events was performed using the following steps. First, we identified the events associated with protons using the ΔE-E cut in the 2D plot of energy loss in the proportional counter (corrected for the trajectory length in the active volume of the proportional counter cells) vs total energy deposited in the silicon detector (see Fig. 21). Second, we calculated the Q-value of the reaction using recoil proton energy, scattering angle and energy of the ^{14}N beam. The two latter values are established from the proton trajectory reconstruction using the position sensitivity of the silicon array and the proportional counters. We then gate on the Q-value of the

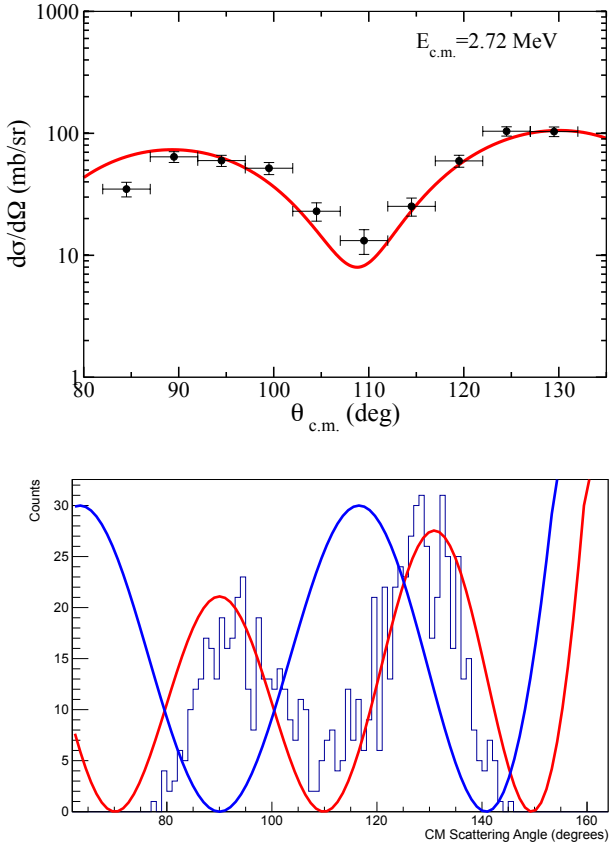

Figure 20: Angular distribution at 2.72 MeV. The solid red curve in the top figure is an R-Matrix fit with 4^+ spin-parity assignment of the resonance at 2.72 MeV. The dramatic difference between the 3^- (blue curve) and the 4^+ (red curve) spin-parity assignments is demonstrated in the bottom figure by comparing the P_3^2 and P_4^2 Legendre polynomials squared to the experimental angular distribution. The upper panel of the figure is adopted from [25].

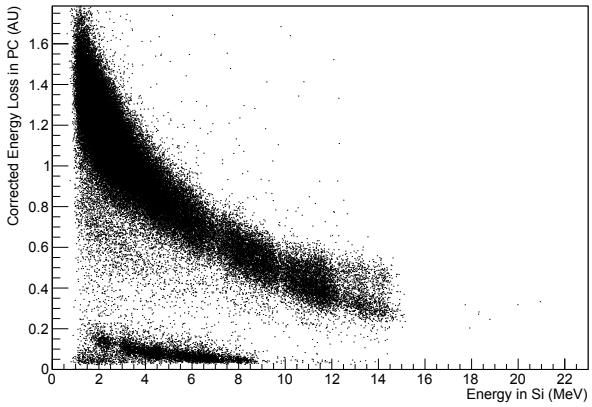

Figure 21: The ΔE-E spectrum showing particle ID for the light recoils. The proton (bottom) and α (top) groups are well separated.

^{14}N(α,p)^{17}O(g.s.) reaction (-0.8 MeV) (see Fig. 22). The Q-value resolution is between 0.9 MeV and 1.1 MeV depending on angle and excitation.

The 2D plot of energy vs angle dependence, shown in Fig. 23 for the selected events, clearly demonstrates kinematic bands that correspond to the ^{18}F excited states observed in ^{14}N(α,p)^{17}O(g.s.) reaction. Gaps in the spectrum are associated with the gaps between the groups of Si detectors. The excitation function for the ^{14}N(α,p)^{17}O(g.s.) reaction measured by the forward segment of ANASEN detector is shown in Fig. 24. It is scaled to compare to the direct kinematics measurement with an implanted ^{14}N target [29]. (No accurate absolute normalization was performed in this stable beam test run.) There is also good data on the ground state branch from the time-reverse reaction ^{17}O(p,α) [28] that covers narrow excitation energy of ^{18}F from 7.2 MeV to 8.2 MeV. All major resonances observed in [28] using traditional direct kinematics measurements can be clearly identified. The energy resolution of the (α,p) spectrum was measured by ANASEN to be 80 keV in c.m. for $\theta_{lab} < 25°$. The energy resolution is observed to degrade at larger laboratory angles, and changes are being implemented to improve the performance at large angles.

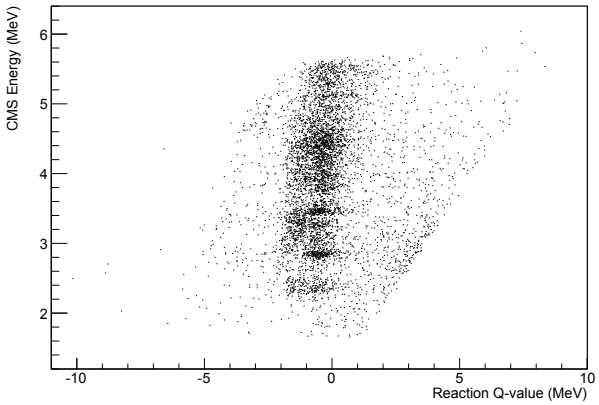

Figure 22: CM energy of recoil protons vs reaction Q-value calculated from the scattering angle and energy of the recoil proton under the assumption of binary kinematics and ^{14}N+α entrance channel. The vertical band at -0.8 MeV corresponds to the ^{14}N(α,p)^{17}O(g.s.) reaction.

6. Conclusion

The new detector, Array for Nuclear Astrophysics and Structure with Exotic Nuclei (ANASEN) has been constructed and commissioned for experiments with rare isotope beams that target nuclear astrophysics and structure of exotic nuclei. We described the general outline and each component of the detector individually. The detector can be used as a stand alone Si+CsI array with zero degrees ionization chamber and as an active target detector, providing high efficiency and tracking capabilities for experiments with low intensity beams of exotic ions. The performance of the detector in active target mode was tested by measuring the α(^{6}He,α) and ^{14}N(α,p)^{17}O(g.s.) excitation func-

tions and comparing the results to the previously available experimental data. An important feature of this detector is that the high ionization beam axis region is naturally isolated and therefore future high-intensity FRIB radioactive beams can also be used with ANASEN in active target mode without any further modification. We expect that this detector will be used extensively with the rare isotope beams provided by ReA3(6) at NSCL or RESOLUT at Florida State University to explore structure of exotic nuclei, and to constrain reactions relevant for nuclear astrophysics using direct and indirect methods.

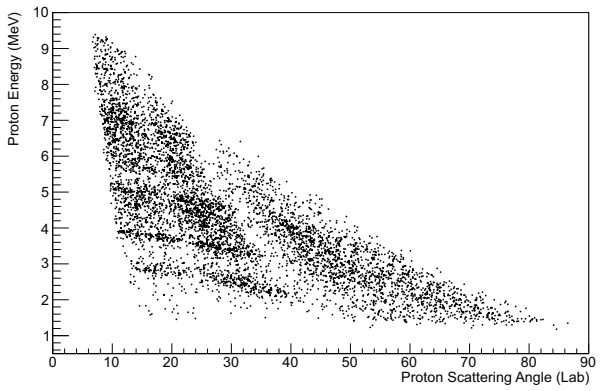

Figure 23: Kinematic dependence of recoil protons energy on scattering angle after the reaction Q-value cut.

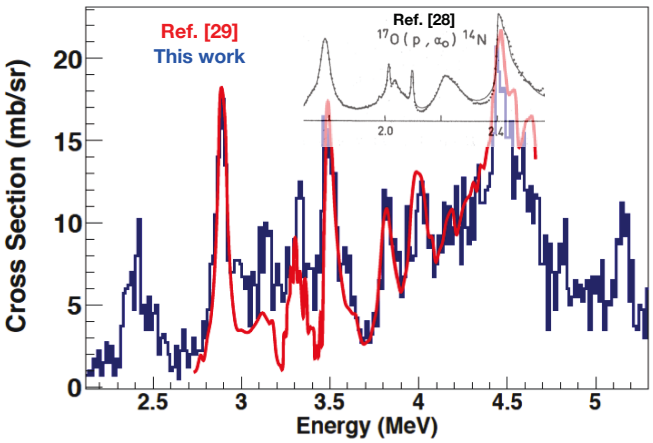

Figure 24: Excitation function for the ^{14}N(α,p)^{17}O(g.s.) for forward detectors compared to the data from [29] and the data on time-reverse reaction ^{17}O(g.s.)(p,α)^{14}N from [28]. The integrated ^{14}N beam flux is about 2×10^{11} ions.

Acknowledgements

ANASEN detector was funded by a Major Research Instrumentation (MRI) Grants No. PHY-0821308 and PHY-0820941 awarded by the National Science Foundation (NSF) to Louisiana State University and Florida State University. This work was also partially supported by NSF Grant No. PHY-456463. The authors G.V.R. and E.K. acknowledge partial support by the U.S. Department of Energy, Office of Science, Office of Nuclear Science, under Award No. DE-FG02-93ER40773. The author G.V.R.also acknowledge the support of the Welsh Foundation (Grant. No. A-1853).

[1] I. Wiedenhöver, L.T. Baby, D. Santiago-Gonzalez, A. Rojas, J.C. Blackmon, G.V. Rogachev, J. Belarge, E. Koshchiy, A.N. Kuchera, L.E. Linhardt, J. Lai, K.T. Macon, M. Matos, and B.C. Rascol. Studies of Exotic Nuclei at the RESOLUT Facility of Florida State University. *Proceedings of the 5th International Conference on "Fission and properties of neutron-rich nuclei" (ICFN5)*, pages 144–151, 2014.

[2] A. M. Laird, P. Amaudruz, L. Buchmann, S. P. Fox, B. R. Fulton, D. Gigliotti, T. Kirchner, P. D. Mumby-Croft, R. Openshaw, M. M. Pavan, J.Pearson, G. Ruprecht, G. Sheffer, and P. Walden. Status of TACTIC: A detector for nuclear astrophysics . *Nuclear Instruments and Methods in Physics Research Section A: Accelerators, Spectrometers, Detectors and Associated Equipment*, 573(12):306 – 309, 2007. Proceedings of the 7th International Conference on Position-Sensitive DetectorsPSD-77th International Conference on Position-Sensitive Detectors.

[3] S. D. Pain, D. W. Bardayan, J. C. Blackmon, K. Y. Chae, K. A. Chipps, J. A. Cizewski, R. Hatarik, M. S. Johnson, K. L. Jones, R. Kapler, R. L. Kozub, R. J. Livesay, C. Matei, B. H. Moazen, C. D. Nesaraja, P. O'Malley, M. S. Smith, T. Swan, J. S. Thomas, and G. L. Wilson. Development of ORRUBA: A Silicon Array for the Measurement of Transfer Reactions in Inverse Kinematics. In *Proc. 4th. Intern. Conf. Fission and Properties of Neutron-Rich Nuclei*, 2008.

[4] Wayne Faszer. Window material test. `http://lin12.triumf.ca/stinson/faszer_report2.ps`, 2003.

[5] Laura Pratt. Study of ^{18}Ne Using the Array for Nuclear Astrophysics and Structure with Exotic Nuclei. `http://etd.lsu.edu/docs/available/etd-04142014-132956/unrestricted/PrattDissertation3.pdf`, 2014.

[6] Rob Veenhof. GARFIELD: computer code. `http://garfield.web.cern.ch/garfield`, 1998.

[7] D. Ohsawa, S. Masaoka, R. Katano, and Y. Isozumi. Resolution of a position-sensitive proportional-counter with a resistive anode wire of carbon fiber. *Applied Radiation and Isotopes*, 52(4):943 – 954, 2000.

[8] G. P. Westphal, H. Pirker, and C. M. Fleck. A new pulse dividing circuit and its application to a position sensitive 10BF3 proportional counter. *Nuclear Instruments and Methods*, 96(2):333 – 339, 1971.

[9] G. L. Miller, N. Williams, A. Senator, R. Stensgaard, and J. Fischer. A position sensitive detector for a magnetic spectrograph. *Nuclear Instruments and Methods*, 91(3):389 – 396, 1971.

[10] V. Radeka. Signal, Noise and Resolution in Position-Sensitive Detectors . *IEEE Transactions on Nuclear Science*, 21(1):51–64, 1971.

[11] K. Hasegawa, K. Mochiki, M. Koike, Y. Satow, H. Hashizume, and Y. Iitaka. High-count rate position-sensitive detectors for synchrotron radiation experiments. *Nuclear Instruments and Methods in Physics Research Section A: Accelerators, Spectrometers, Detectors and Associated Equipment*, 252(23):158 – 168, 1986.

[12] F. Bird, S. Shapiro, V. Ashford, D. McShurley, R. Reif, D. W.G.S. Leith, and S. Williams. Charge Division Using Carbon Filaments for Obtaining Coordinate Information from Detection of Single Electrons . *IEEE Transactions on Nuclear Science*, 33(1):261 – 266, 1986.

[13] D. Ohsawa, R. Katano, Y. Ito, and Y. Isozumi. A simple crystal spectrometer for low-energy photons emitted from radioactive sources, Part {II} . *Nuclear Instruments and Methods in Physics Research Section A: Accelerators, Spectrometers, Detectors and Associated Equipment*, 390 (12):183 – 190, 1997.

[14] T. Iwazumi, K. Kobayashi, S. Kishimoto, T. Nakamura, S. Nanao, D. Ohsawa, R. Katano, and Y. Isozumi. Magnetic resonance effect in x-ray resonant raman scattering. *Phys. Rev. B*, 56:R14267–R14270, 1997.

[15] T. Nakamura, S. Nanao, T. Iwazumi, K. Kobayashi, S. Kishimoto, D. Ohsawa, R. Katano, and Y. Isozumi. X-ray magnetic circular dichroism of multielectron excitation by fluorescence spectroscopy. *Journal of Electron Spectroscopy and Related Phenomena*, 92(13):261 – 264, 1998.

[16] G. L. Engel, M. Sadasivam, M. Nethi, J. M.Elson, L. G. Sobotka, and R. J. Charity. A multi-channel integrated circuit for use in low- and

intermediate-energy nuclear physics - hinp16c. *Nuclear Instruments and Methods in Physics Research Section A: Accelerators, Spectrometers, Detectors and Associated Equipment*, 573(3):418 – 426, 2007.

[17] NSCL Data Acquisition. `http://docs.nscl.msu.edu/daq/index.php`.

[18] B. Davin, R. T de Souza, R. Yanez, Y. Larochelle, R. Alfaro, H. S Xu, A. Alexander, K. Bastin, L. Beaulieu, J. Dorsett, G. Fleener, L. Gelovani, T. Lefort, J . Poehlman, R. J. Charity, L. G. Sobotka, J. Elson, A. Wagner, T. X. Liu, X. D. Liu, W. G. Lynch, L. Morris, R. Shomin, W. P. Tan, M. B. Tsang, G. Verde, and J. Yurkon. LASSA: a large area silicon strip array for isotopic identification of charged particles. *Nuclear Instruments and Methods in Physics Research Section A: Accelerators, Spectrometers, Detectors and Associated Equipment*, 473(3):302 – 318, 2001.

[19] G Charpak and F Sauli. High-resolution electronic particle detectors. *Annual Review of Nuclear and Particle Science*, 34(1):285–350, 1984.

[20] A Romaniuk. Atlas note. *ATL-INDET-98-211*, 1998.

[21] J. A. Sawicki, B. D. Sawicka, and J. Stanek. Conversion electron mössbauer spectroscopy at low temperatures. *Nuclear Instruments and Methods*, 138(3):565 – 566, 1976.

[22] Y. Isozumi, M. Kurakado, and R. Katano. A proportional counter for resonance-electron Mössbauer spectroscopy at low temperatures down to 77.3 K . *Nuclear Instruments and Methods in Physics Research*, 204(23): 571 – 575, 1983.

[23] Daniel Santiago-Gonzales. Experimental Investigation on the Nuclear Structure of the Neutron-rich Nuclides ^{44}S and ^{20}O. `https://publications.nscl.msu.edu/thesis/Santiago-Gonzalez2014_367.pdf`, 2013.

[24] D. Suzuki, A. Shore, W. Mittig, J. J. Kolata, D. Bazin, M. Ford, T. Ahn, F. D. Becchetti, S. Beceiro Novo, D. Ben Ali, B. Bucher, J. Browne, X. Fang, M. Febbraro, A. Fritsch, E. Galyaev, A. M. Howard, N. Keeley, W. G. Lynch, M. Ojaruega, A. L. Roberts, and X. D. Tang. Resonant α scattering of ^{6}He: Limits of clustering in ^{10}Be. *Phys.Rev. C*, 87:054301, 2013.

[25] Anthony Nicholas Kuchera. Clustering Phenomena in the a=10 T=1 Isobaric Multiplet. `http://diginole.lib.fsu.edu/etd/8585:ElectronicThesis,TreatisesandDissertations.Paper8585`, 2013.

[26] N. Curtis, D. D. Caussyn, N. R. Fletcher, F. Marechal, N. Fay, and D. Robson. Decay Angular Correlations and Spectroscopy for ^{10}Be$^{*} \rightarrow$ ^{4}He + ^{6}He. *Phys.Rev.*, C64:044604, 2001.

[27] M. Freer, E. Casarejos, L. Achouri, C. Angulo, N. I. Ashwood, N. Curtis, P. Demaret, C. Harlin, B. Laurent, M. Milin, N. A. Orr, D. Price, R. Raabe, N. Soic, and V. A. Ziman. α:2n:α Molecular Band in ^{10}Be. *Phys.Rev.Lett.*, 96:042501, 2006.

[28] J. C. Sens, S. M. Refaei, and A. Pape. Search for Simple Configurations in ^{18}F. II. The ^{17}O(p, α_0)^{14}N, ^{17}O(p, p$_1\gamma$)^{17}O, and ^{17}O(p, γ)^{18}F Reactions. *Phys.Rev.*, C18:2007, 1978.

[29] J. Terwagne, G. Genard, M. Yedji, and G. G. Ross. Cross-section Measurements of the ^{14}N(α,p)^{17}O and ^{14}N(α,α)^{14}N Reactions between 3.5 and 6 MeV. *Journal of Applied Physics*, 104:084909, 2008.